Impact of Airflow Rate on Amplitude and Regional Distribution of Normal Lung Sounds

Elmar Messner[1], Martin Hagmüller[1], Paul Swatek[2], Freyja-Maria Smolle-Jüttner[2] and Franz Pernkopf[1]

[1]*Signal Processing and Speech Communication Laboratory, Graz University of Technology, Graz, Austria*

[2]*Division of Thoracic and Hyperbaric Surgery, Medical University of Graz, Graz, Austria*

Keywords: Lung Sounds, Multichannel Recording, Respiratory Flow, Acoustic Thoracic Images.

Abstract: In computerized lung sound research, the usage of a pneumotachograph, defining the phase of respiration and airflow velocity, is essential. To obviate its need, the influence of airflow rate on the characteristics of lung sounds is of great interest. Therefore, we investigate its effect on amplitude and regional distribution of normal lung sounds. We record lung sounds on the posterior chest of four lung-healthy male subjects in supine position with a 16-channel lung sound recording device at different airflow rates. We use acoustic thoracic images to discuss the influence of airflow rate on the regional distribution. At each airflow rate, we observe louder lung sounds over the left hemithorax and a constant regional distribution above an airflow rate of 0.7 l/s. Furthermore, we observe a linear relationship between the airflow rate and the amplitude of lung sounds.

1 INTRODUCTION

In auscultation, beside distinct findings like adventitious lung sounds, also the lung sound intensity is used as a diagnostic marker. For example, physicians examine the differences in intensity between left- and right-sided lung sounds at pneumothorax condition. Therefore, a basic knowledge about the regional distribution of normal lung sound intensity, but also its dependence on airflow rate is essential. Moreover, a good understanding of this dependence could render the pneumotachograph dispensable for lung sound research, because of airflow estimation directly from lung sounds.

Several research groups already investigated the effect of airflow rate on the amplitude and the regional distribution of lung sound. Differing relationships were observed in (Kraman, 1984), (Gavriely and Cugell, 1996), (Hossain and Moussavi, 2002) and (Shykoff et al., 1988). Recently, the authors in (Yosef et al., 2009) showed the effect of airflow rate on Vibration Response Imaging measurement in healthy lungs during expiration, but also discussed the relationship between lung sound energy and airflow rate. The authors in (Torres-Jimenez et al., 2008a) used a 5x5 microphone array and generated respiratory acoustic thoracic images (RATHI) to discuss the regional distribution of lung sounds, by comparing its performance with clinical physicians. In (Torres-Jimenez et al., 2008b), the authors further show RATHIs at different airflow rates.

In this paper, we independently investigate the impact of airflow rate on amplitude and regional distribution of normal lung sounds. For that, we recorded lung sounds on the posterior chest of four lung-healthy male subjects with a 16-channel lung sound recording device (Messner et al., 2016) at airflow rates of 0.3, 0.7, 1.0, 1.3 and 1.7 l/s during inspiration. In contrast to other research groups, we recorded lung sounds in supine position. Another differentiation is the usage of uncontaminated lung sound recordings, i.e. free of heart and other interfering sounds. By means of acoustic thoracic images (Charleston-Villalobos et al., 2004), we discuss the regional distribution of lung sounds dependent on airflow rate. To generate the surface acoustic thoracic images from the multiple lung sound signals, we use 2D-interpolation. For each subject, we illustrate the acoustic thoracic images at the five airflow rates independently. We observe a constant regional distribution above an airflow rate of 0.7 l/s. Furthermore, we observe a linear relationship between the airflow rate and the amplitude of lung sounds. Our results most closely correspond to the findings in (Yosef et al., 2009) and are independent of the recording position.

We organized the paper as follows. Section 2 de-

Messner E., HagmÃijller M., Swatek P., Smolle-JÃijttner F. and Pernkopf F.
Impact of Airflow Rate on Amplitude and Regional Distribution of Normal Lung Sounds.
DOI: 10.5220/0006134400490053
In *Proceedings of the 10th International Joint Conference on Biomedical Engineering Systems and Technologies (BIOSTEC 2017)*, pages 49-53
ISBN: 978-989-758-212-7

scribes the data acquisition, the subjects, the recording material, the signal pre-processing and the generation of the acoustic thoracic images. Section 3 presents our observations for the regional distribution and the lung sound amplitude for different airflow rates. In Section 4, we discuss the results and Section 5 concludes the paper.

2 MATERIALS AND METHODS

2.1 Data Acquisition

We recorded the lung sounds with a multichannel recording device, which enables the simultaneous recording of airflow (Messner et al., 2016). The device is equipped with a multichannel lung sound recording front-end and a pneumotachograph.

The recording front-end is a foam pad covered with artificial leather, a similar construction as the Stethographics STG 16 (Murphy, 2007). On the surface of the pad, we arranged 16 lung sound transducers (LSTs) with a fixed pattern. The pattern is comparable with the one proposed in (Sen and Kahya, 2006). Based on the approach with air-coupled electret-

Figure 1: Multichannel recording front-end of the lung sound recording device (Messner et al., 2016). 16 lung sound transducers are distributed on the foam pad. The center line represents the spine.

condenser microphones (Pasterkamp et al., 1993), we modified Littmann Classic II chest pieces for the LST design. By placing the foam pad under the back of the subject, we perform the recording of the lung sounds in supine position on an examination table.

We use standard audio recording equipment for the analogue pre-filtering, pre-amplification, and digitization of the LST signals. The sampling frequency is $f_s = 16$ kHz and the resolution is 24 bit. Before the analog-to-digital conversion of the LST signals, we apply a Bessel high-pass filter with a cut-off frequency of $f_c = 80$ Hz and a slope of 24 dB/oct.

We measure the airflow with a pneumotachograph Schiller SP 260. The airflow signal is sampled with a frequency $f_s = 400$ Hz.

We calibrate the recording device with a Brüel & Kjær sound calibrator Type 4231, a sound source with a sinusoidal waveform at a frequency of $f = 1$ kHz and with a sound pressure level of 94 dB. We adjusted the microphone preamplifiers of the LSTs to reach the same signal level for the sound calibrator.

2.2 Subjects and Material

At airflow rates of 0.3, 0.7, 1.0, 1.3 and 1.7 l/s, we recorded lung sounds over the posterior chest of four lung-healthy subjects. The subjects held the pneumotachograph with both hands and wore a nose clip. The subjects breathe steadily during inspiration at the given airflow rates and with natural breathing during expiration. The recording setup provided a real-time feedback for the airflow rate. The subjects were placed on the pad with a defined distance $d \approx 7$ cm between the 7th cervical vertebra (C7) and the center line of the topmost row of sensors. The recording material of one subject consists of 16-channel lung sound recordings at five different airflow rates, with 4-8 breathing cycles within 30 seconds, respectively. The subjects were four male volunteers, with no diagnosed lung diseases and with the following metadata: age (27, 27, 26, 27 years), weight (78, 75, 75, 75 kg) and height (1.8, 1.78, 1.89, 1.72 m).

The used multichannel recording front-end is robust against ambient noise. However, in lung sound recordings, interfering signals are caused by the heart, bowels and body movement. These can distort the signal energy values from lung sound signals. To ensure uncontaminated lung sound recordings, we manually labeled the sections containing heart, bowel and other interfering sounds.

2.3 Signal Pre-processing

We applied a bandpass filter, with a lower cut-off frequency $f_L = 150$ Hz and an upper cut-off frequency $f_H = 250$ Hz, to the 16 lung sound signals. To calculate the energy, we used a sliding window with a length of 50 ms and an overlap of 75 %.

2.4 Acoustic Thoracic Images

To illustrate the regional distribution of the lung sound energy, we use acoustic thoracic images. We generate the images for the left and the right hemithorax independently. In particular, we use the energy signal of the left-sided (Sensors 3, 4, 7, 8, 11, 12, 15 and 16) and right-sided sensors (Sensors 1, 2, 5, 6, 9, 10, 13 and 14), respectively. To generate an acoustic thoracic image at a certain airflow rate, we used the appropriate segments of the recording. We average the energy values of all the uncontaminated segments, i.e. labeled as free of interfering sounds (cf. Section 2.2), where the subjects reached the proper airflow rate. For the interpolation between the energy values, obtained from the eight sensor signals, we use the biharmonic spline interpolation. The resulting acoustic thoracic images are grayscale images (see Figure 4). The white color indicates the minimum value and the black color the maximum value.

3 RESULTS

3.1 Amplitude

Figure 2 shows the square root of the sound energy as a function of airflow rate for all of the four subjects independently. We performed linear regression for the values from each subject independently (The results are not shown in Figure 2).

For Subject 1, the coefficient of determination is $R^2 = 0.98$, for Subject 2 it is $R^2 = 0.96$, for Subject 3 it is $R^2 = 0.99$ and for Subject 4 it is $R^2 = 0.99$. Figure 3 shows the spectral characteristics (i.e. power spectral density (PSD)) of the lung sounds at different airflow rates, generated from the lung sound recording of the sensor at position 6 (see Figure 1) from Subject 1.

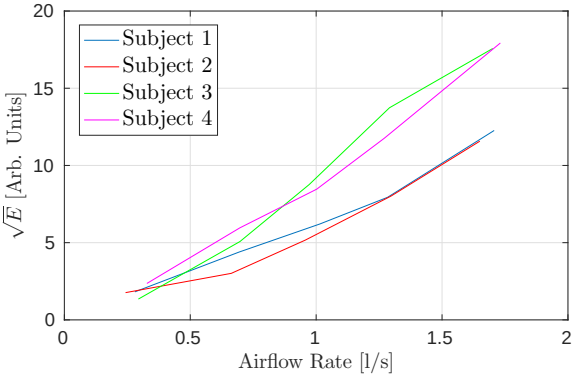

Figure 2: Square root of the sound energy $\sqrt{E}$ as a function of airflow rate for all four subjects.

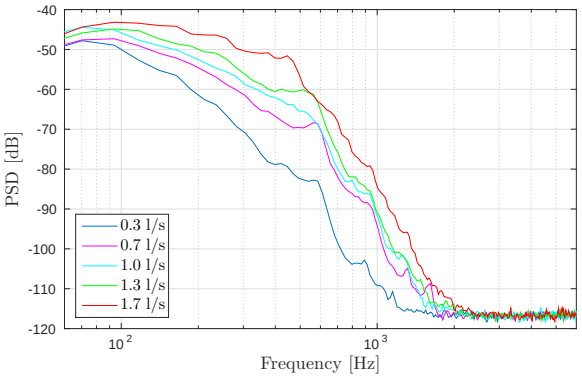

Figure 3: Spectral characteristics of the lung sounds at different airflow rates, generated from the lung sound recording of the sensor at position 6 (see Figure 1) from Subject 1.

3.2 Regional Distribution

Figure 4 shows the acoustic thoracic images of four lung-healthy subjects, evaluated at five different airflow rates. The grayscale images are normalized for the respective airflow rate. For an airflow rate of 0.3 l/s, we observe that most of the energy is in the middle right area. Already for an airflow rate of 0.7 l/s, the lung sound energy is higher towards the base of the lungs. Above an airflow rate of 0.7 l/s, the regional distribution remains almost constant.

Table 1 shows the mean and standard deviation of the percentage of the summed up energy from the sensors over the left, right, upper (sensor 1 to 8) and lower hemithorax (sensor 9 to 16). The signal energy over the left lung is distinctly higher than over the right lung. This is further reflected in the acoustic thoracic images, especially above an airflow rate of 0.3 l/s. The values in Table 1 show that with increasing airflow rate the percentage for the left lung increases. Regarding the ratio of the upper to lower hemithorax, for an airflow value of 0.3 l/s the energy in the upper lungs is higher. With increasing airflow, the percentage for the lower lung increases, but for 1.7 l/s it decreases again.

Table 1: Mean and standard deviation of the percentage of the summed up energy from the sensors over the left, right, upper and lower hemithorax for different airflow values.

	0.3 l/s	0.7 l/s	1.0 l/s	1.3 l/s	1.7 l/s
Left	53±8	62±9	59±3	62±3	65±7
Right	47±8	38±9	41±3	38±3	35±7
Upper	56±13	43±5	34±3	33±4	40±1
Lower	44±13	57±5	66±3	67±4	60±1

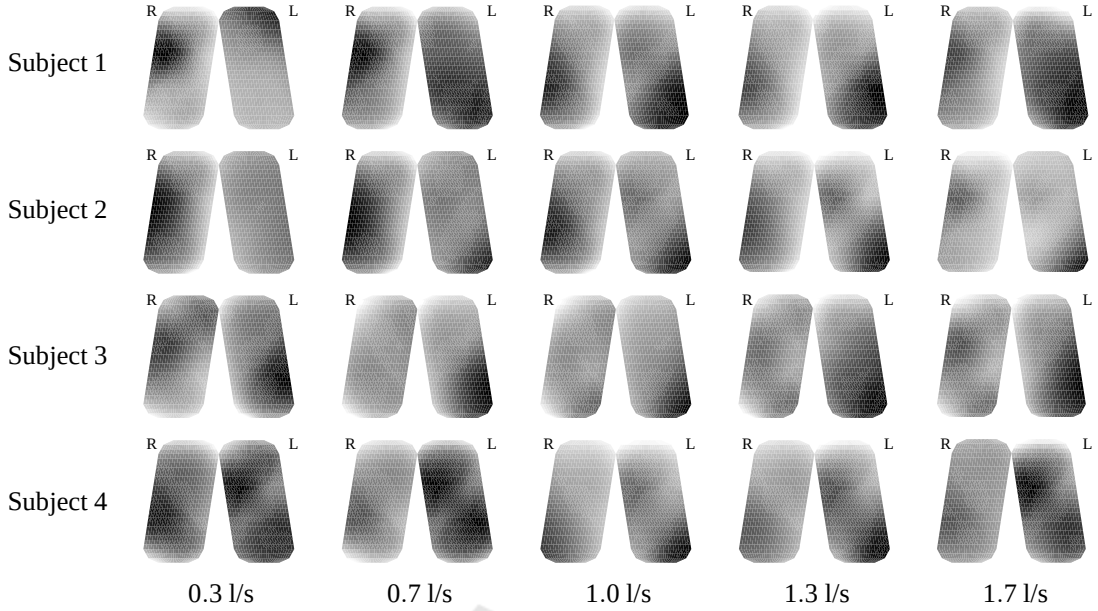

Figure 4: Acoustic thoracic images from four lung-healthy subjects, evaluated at five different airflow rates. The orientation is indicated by the capital letters *R* (right hemithorax) and *L* (left hemithorax).

4 DISCUSSION

To compare our findings with those in (Yosef et al., 2009), we used a similar bandpass filter, with a lower cut-off frequency $f_L = 150$ Hz and an upper cut-off frequency $f_H = 250$ Hz (see Section 2.3). Although we lose important information from the signal in the higher frequency range, due to the dominance of the signal energy in the low frequency range, a higher upper cut-off frequency f_H would not have a huge impact on the acoustic thoracic images. According to Figure 3 a bandpass filter with an upper cut-off frequency of $f_H \approx 600$ Hz could be considered.

Our findings regarding amplitude and regional distribution of lung sounds correspond most closely with those in (Yosef et al., 2009), although we recorded the lung sounds in supine position. The authors in (Fiz et al., 2008) already observed that, compared with sitting, the supine position does not cause a substantial change in lung sound intensity. The authors in (Torres-Jimenez et al., 2008b) also observed a constant regional distribution for RATHIs at airflow rates of 1.0, 1.5 and 2.0 l/s. The authors in (Yosef et al., 2009) showed the same for Vibration Response Images at airflow rates of 1.0, 1.3 and 1.7 l/s. Regarding the relationship between airflow rate and the square root of lung sound energy (see Section 3.1), the authors in (Yosef et al., 2009) achieved for linear regression a coefficient of determination of $R^2 = 0.95$.

A limitation of our experiment is the small number of subjects $n = 4$ and the lack of female subjects.

5 CONCLUSIONS

In this paper, we investigate the impact of airflow rate on amplitude and regional distribution of normal lung sounds. Therefore, we record lung sounds with a multichannel recording device at different airflow rates. We illustrate the regional distribution with acoustic thoracic images.

We observe a linear dependence between airflow rate and lung sound amplitude. In our recordings, the signal energy from lung sounds over the left lung is distinctly higher than from those over the right lung. Above an airflow rate of 0.7 l/s, we observe a constant regional distribution for the lung sound energy. Although we recorded lung sounds on the posterior chest in supine position instead of sitting, our findings match most closely with those in (Yosef et al., 2009).

The observed relationship can be used for the extraction of the airflow from lung sounds. Furthermore, the findings are helpful for future work, regarding the standardized recording of lung sounds and subsequent classification by means of machine learning techniques.

ACKNOWLEDGEMENTS

This project was supported by the government of Styria, Austria, under the project call HTI:Tech_for_Med. The authors acknowledge 3M™ for providing Littmann® stethoscope chest pieces and Schiller AG for the support with a spirometry solution.

REFERENCES

Charleston-Villalobos, S., Cortés-Rubiano, S., González-Camerena, R., Chi-Lem, G., and Aljama-Corrales, T. (2004). Respiratory acoustic thoracic imaging (RATHI): assessing deterministic interpolation techniques. *Medical and Biological Engineering and Computing*, 42(5):618–626.

Fiz, J. A., Gnitecki, J., Kraman, S. S., Wodicka, G. R., and Pasterkamp, H. (2008). Effect of body position on lung sounds in healthy young men. *CHEST Journal*, 133(3):729–736.

Gavriely, N. and Cugell, D. W. (1996). Airflow effects on amplitude and spectral content of normal breath sounds. *Journal of applied physiology*, 80(1):5–13.

Hossain, I. and Moussavi, Z. (2002). Relationship between airflow and normal lung sounds. In *Proceedings of the 15th IEEE Canadian Conference on Electrical and Computer Engineering (CCECE'02)*, pages 1120–1122.

Kraman, S. (1984). The relationship between airflow and lung sound amplitude in normal subjects. *CHEST Journal*, 86(2):225–229.

Messner, E., Hagmüller, M., Swatek, P., and Pernkopf, F. (2016). A robust multichannel lung sound recording device. In *Proceedings of the 9th Annual International Conference on Biomedical Electronics and Devices (BIODEVICES'16)*, pages 34–39.

Murphy, R. (2007). Development of acoustic instruments for diagnosis and management of medical conditions. *Engineering in Medicine and Biology Magazine*, 26(1):16–19.

Pasterkamp, H., Kraman, S., DeFrain, P., and Wodicka, G. (1993). Measurement of respiratory acoustical signals. Comparison of sensors. *CHEST Journal*, 104(5):1518–1525.

Sen, I. and Kahya, Y. (2006). A multi-channel device for respiratory sound data acquisition and transient detection. In *Proceedings of the 27th Annual International Conference of the IEEE Engineering in Medicine and Biology Society (EMBS'06)*, pages 6658–6661.

Shykoff, B. E., Ploysongsang, Y., and Chang, H. (1988). Airflow and normal lung sounds1. 2. *Am Rev Respir Dis*, 137:872–876.

Torres-Jimenez, A., Charleston-Villalobos, S., Gonzalez-Camarena, R., Chi-Lem, G., and Aljama-Corrales, T. (2008a). Asymmetry in lung sound intensities detected by respiratory acoustic thoracic imaging (RATHI) and clinical pulmonary auscultation. In *Proceedings of the 30th Annual International Conference of the IEEE Engineering in Medicine and Biology Society (EMBS'08)*, pages 4797–4800.

Torres-Jimenez, A., Charleston-Villalobos, S., Gonzalez-Camarena, R., Chi-Lem, G., and Aljama-Corrales, T. (2008b). Respiratory acoustic thoracic imaging (RATHI): Assessing intrasubject variability. In *Proceedings of the 30th Annual International Conference of the IEEE Engineering in Medicine and Biology Society (EMBS'08)*, pages 4793–4796.

Yosef, M., Langer, R., Lev, S., and Glickman, Y. A. (2009). Effect of airflow rate on vibration response imaging in normal lungs. *The open respiratory medicine journal*, 3(1).